 doi:10.20944/preprints202103.0745.v1

Article

Machine learning-based pulse wave analysis for early detection of abdominal aortic aneurysms using *in silico* pulse waves

Tianqi Wang [1,2], Weiwei Jin [1], Fuyou Liang [2,3] and Jordi Alastruey [1,3,*]

[1] Department of Biomedical Engineering, School of Biomedical Engineering and Imaging Sciences, King's College London, London, UK
[2] School of Naval Architecture, Ocean and Civil Engineering, Shanghai Jiao Tong University, Shanghai, China
[3] World-Class Research Center "Digital Biodesign and Personalized Healthcare", Sechenov First Moscow State Medical University, Moscow, Russia
* Correspondence: jordi.alastruey-arimon@kcl.ac.uk

Abstract: An abdominal aortic aneurysm (AAA) is usually asymptomatic until rupture, which is associated with extremely high mortality. Consequently, early detection of AAAs is of paramount importance in reducing mortality; however, most AAAs are detected by medical imaging incidentally. The aim of this study was to investigate the feasibility of machine learning-based pulse wave (PW) analysis for the early detection of AAAs using a database of *in silico* PWs. PWs in the large systemic arteries were simulated using one-dimensional blood flow modelling. A database of *in silico* PWs representative of subjects (aged 55, 65 and 75 years) with different AAA sizes was created by varying the AAA-related parameters with major impacts on PWs – identified by parameter sensitivity analysis – in an existing database of *in silico* PWs representative of subjects without AAA. Then, a machine learning architecture for early detection of AAAs was proposed, which was trained and tested using the new *in silico* PW database. The parameter sensitivity analysis revealed that the AAA maximum diameter and stiffness of the large systemic arteries were the dominant AAA-related biophysical properties that significantly influence the PW. The simulated PW indexes extracted from the database showed that the PW was not only influenced by the presence of an AAA but was also significantly affected by multiple cardiovascular parameters that compromised the detection of AAAs by using individual PW indexes. Alternatively, the trained machine learning model performed well in classifying normal and AAA conditions using digital photoplethysmogram PWs from the database. These findings suggest that machine learning-based PW analysis is a promising approach for AAA screening using PW signals acquired by wearable devices.

Keywords: abdominal aortic aneurysm; pulse wave analysis; one-dimensional modelling; *in silico* pulse waves; machine learning; recurrent neural network; long short-term memory

1. Introduction

An abdominal aortic aneurysm (AAA) is usually defined as the irreversible localized dilatation of the infrarenal abdominal aorta, which is usually asymptomatic until rupture [1]. The morbidity of AAA is significantly higher in men than in women (1.3% to 8.9% vs. 1.0% to 2.2%) and increases as a result of various factors such as tobacco smoking, ageing, and family history of AAAs [1-3]. Given that the rupture of an AAA is often lethal with the mortality reaching about 90% [4,5], timely diagnosis and appropriate treatment are crucial for patients with an AAA. Large AAAs in thin people can often be detected by physical examination, but the accuracy depends on the examiner's skills and considerably reduces for the obese body habitus and small AAA size [6]. In current clinical practice, AAAs are most often detected as incidental findings of ultrasonography, abdominal computed tomography, or magnetic resonance imaging performed for other purposes [6]. However, these medical imaging examinations require professional equipment that cannot be used in daily life.

Preprints (www.preprints.org) | NOT PEER-REVIEWED | Posted: 30 March 2021 doi:10.20944/preprints202103.0745.v1

Considering that the presence of an AAA has a systemic impact on the biophysical properties of the cardiovascular system, thus influencing the arterial pulse wave (PW) [7,8], PW analysis may provide an alternative approach to the early detection of AAAs using wearable devices. These are more convenient and less expensive for large-scale screening than medical imaging exams. In particular, the photoplethysmogram (PPG) PW is easily acquired using pulse oximeters, which are frequently used in healthcare to measure arterial blood oxygen saturation and pulse rate. The PPG signal can also be acquired by devices available to the wider population, such as smartphones, smartwatches and fitness bands [9]. Therefore, if it was possible to detect an AAA from the PPG then it may have great clinical utility.

In recent years, machine learning-based PW analyses have been performed to investigate a wide range of clinical problems, showing promising results [10-13]. Training machine learning models usually requires databases of PWs measured in a large number of subjects. Acquiring these data, however, presents several challenges: (i) measurement accuracy is subject to the type of equipment used and may be operator-dependent; (ii) it is complex to measure PWs at all sites of interest; (iii) it can be difficult to measure reference variables precisely; (iv) it is challenging to study the influence of individual cardiovascular properties on the PW *in vivo* since other properties may change over time; and (v) data acquisition is expensive and time-consuming. Databases of simulated PWs representative of samples of real subjects provide an alternative approach that addresses all these challenges. A database of *in silico* PWs can be produced by using computational blood flow modelling [14-17]. This is a cost-effective approach to generate a large number of virtual subjects, each with a distinctive set of PW signals, across a wide range of pathophysiological conditions for the training process of a machine learning model for PW analysis. Consequently, machine learning-based PW analysis using the database of *in silico* PWs could be employed for the early detection of AAAs.

Previous studies on AAAs have mainly studied AAA rupture by statistical analysis of AAA morphology [18,19], biomechanical analysis using semi-empirical equations [20], and three-dimensional finite element analysis of AAA wall stress [21,22]. Some computational studies investigated the initiation and growth of an AAA [23-25], and others focused on the prediction and planning of interventional procedures for AAAs such as endovascular deployment of stent-grafts [26-28]. Moreover, some studies have studied PW propagation in the presence of AAA [29-31] and a few studies have investigated the effects of AAA on PW morphology by using computational blood flow modelling [32-36].

The aim of this study was to (i) create a new database of *in silico* PWs representative of subjects aged 55, 65 and 75 years old, with and without AAAs, and (ii) further investigate the feasibility of machine learning-based PW analysis for the early detection of AAA using this database. Firstly, PWs in baseline subjects with and without AAAs were modeled using one-dimensional blood flow modelling, and a parameter sensitivity analysis was performed to evaluate the influence of AAA-related biophysical properties on the simulated PWs. Subsequently, the new database of *in silico* PWs was created by introducing the AAA-related parameters found to have a large impact on PWs (by the sensitivity analysis) into an existing *in silico* PW database representative of subjects without AAA [14]. Finally, a machine learning architecture was proposed based on the recurrent neural network (RNN). This was trained and tested using the peripheral PPG PW derived from the *in silico* PW database to evaluate the performance of machine learning-based PW analysis for the early detection of AAAs.

2. Materials and Methods

Preprints (www.preprints.org) | NOT PEER-REVIEWED | Posted: 30 March 2021 doi:10.20944/preprints202103.0745.v1

2.1. Modeling pulse waves in baseline subjects with and without AAAs

One-dimensional blood flow modelling in the lager systemic arteries (see Figure 1) was used to simulate several PW signals: blood pressure, blood flow velocity, blood flow rate, and PPG. The baseline subject without an AAA was adapted from the baseline 65-year-old subject derived from the database of *in silico* PWs developed by Charlton [14], given that it is usually elderly people who suffer from AAA [2,22]. Herein, two biophysical properties of the original model were adapted to make the subjects with and without AAA comparable: (i) the tapered infrarenal abdominal aorta was replaced by a straight tube with a diameter equal to the average value of the original proximal and distal diameters, and (ii) wall viscosity in this segment was removed to improve numerical stability. The baseline subject with an AAA was then obtained by modifying the baseline subject without AAA (Figure 1). First, the shape of the infrarenal abdominal aorta was transformed from a straight line (*i.e.*, constant diameter) into a cosine curve with the same length and the maximum diameter being set at 30 mm. And second, the stiffness of this segment, which was quantified by the product of elastic modulus and wall thickness (*Eh*), was decoupled from the diameter and thereby maintained constant.

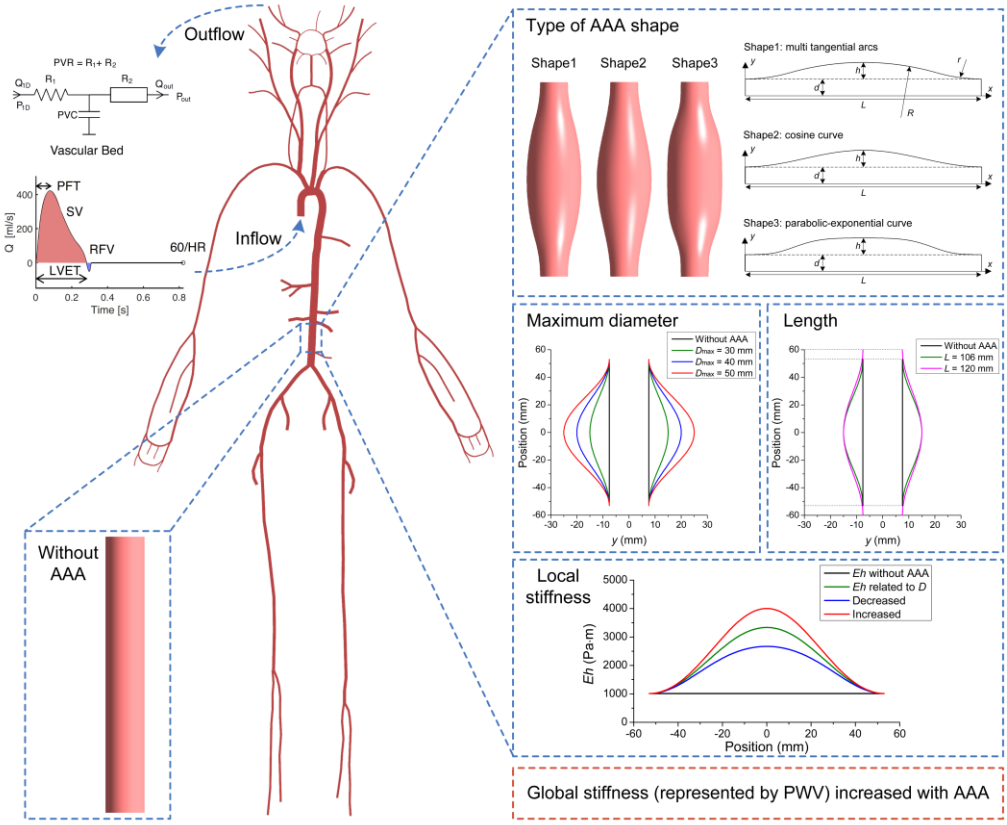

Figure 1. The one-dimensional model of pulse wave propagation with normal infrarenal adominal aorta (left) and the parameter variations considered to simulate an AAA (right). These include 1) type of AAA shape, 2) AAA maximum diameter (D_{max}), 3) AAA length (L), 4) AAA local stiffness (Eh; *i.e.*, elastic modulus multiplied by wall thickness), and 5) global stiffness of the larger systemic arteries. The model contains the arterial segments making up the larger systemic arteries, an aortic inflow waveform prescribed at the aortic root, and lumped outflow boundary conditions at each terminal segment representing vascular beds.

2.2. Parameter sensitivity analysis

Based on the reference model of a subject aged 65 years old with an AAA introduced in Section 2.1, several AAA-related biophysical properties – the type of AAA

Preprints (www.preprints.org) | NOT PEER-REVIEWED | Posted: 30 March 2021 doi:10.20944/preprints202103.0745.v1

shape, AAA maximum diameter, AAA length, AAA local stiffness, and global stiffness of the larger systemic arteries – were varied individually to investigate their influence on the simulated PWs (see Figure 1).

Although AAAs in real patients are usually fusiform and asymmetric [1,21,37], previous model-based studies have simulated AAAs as being axi-symmetrical with a geometry that can be described by several types of mathematical functions [33,35]. In the present study, three common types of AAA shapes derived from previous studies were considered: multiple tangential arcs [33] (Shape 1), a cosine curve [35,38] (Shape 2), and a parabolic-exponential curve [39] (Shape 3) (see Figure 1). The mathematical functions of the radius (y) against the distance from the vessel inlet (x) for the three types of shapes were respectively expressed by

$$\begin{cases} y = r\left(1-\sqrt{1-\dfrac{x^2}{r^2}}\right)+d, \quad 0 \le x \le \dfrac{4hLr}{4h^2+L^2} \\ y = \sqrt{\left(\dfrac{4h^2+L^2}{8h}-r\right)^2-\left(x-\dfrac{L}{2}\right)^2}-\dfrac{L^2-4h^2}{8h}+r+d, \quad \dfrac{4hLr}{4h^2+L^2} < x \le L-\dfrac{4hLr}{4h^2+L^2} \\ y = r\left(1-\sqrt{1-\dfrac{(L-x)^2}{r^2}}\right)+d, \quad L-\dfrac{4hLr}{4h^2+L^2} \le x \le L \\ r = 0.02\dfrac{4h^2+L^2}{4hL} \end{cases}, \tag{1}$$

$$y = d+\frac{h}{2}\left(1+\cos\left(2\pi\left(\frac{x}{L}-\frac{1}{2}\right)\right)\right), \tag{2}$$

$$\begin{cases} y = d+\left(h-\dfrac{c_3}{d}\left(x-\dfrac{L}{2}\right)^2\right)e^{-c_1\left|\frac{x-\frac{L}{2}}{d}\right|^{c_2}} \\ c_1 = 0.001,\ c_2 = \dfrac{4.605}{\left(\dfrac{L}{2d}\right)^{c_1}},\ c_3 = \dfrac{h}{d\left(\dfrac{4L}{5d}\right)^2} \end{cases}, \tag{3}$$

where d is the radius of the straight infrarenal abdominal aorta without AAA, L is the vessel length, and h is the difference between the AAA maximum diameter and d (see Figure 1).

The AAA size is usually evaluated by the maximum diameter (D_{max}) in clinical practice, with D_{max} larger than 30 mm being diagnosed as AAA and D_{max} larger than 50 mm being stratified as a serious AAA [2,40]. Since this study focused on the early detection of AAAs, herein three levels of D_{max} were considered in the parameter sensitivity analysis: 30, 40 and 50 mm. Besides the maximum diameter, the length of an AAA also shows inter-patient difference [18,41], which was considered in the present study by increasing the length of the reference model from 106 to 120 mm (see Figure 1).

Besides these morphological features, the infrarenal abdominal aorta in subjects with an AAA usually has a higher elastic modulus and a thicker vascular wall compared with normal subjects [25,42]. In the model this was simulated by coupling the stiffness Eh of the AAA with the diameter (D, varying along the infrarenal abdominal aorta) using

$$Eh = D\left[k_1\exp\left(k_2 D\right)+k_3\right]. \tag{4}$$

The values of the empirical constants k_1, k_2, and k_3 were taken from a previous study [14]. Variations in AAA local stiffness were described by multiplying the above expression by

Preprints (www.preprints.org) | NOT PEER-REVIEWED | Posted: 30 March 2021 doi:10.20944/preprints202103.0745.v1

a cosine function that made the maximum *Eh* value decrease or increase by 20% (see Figure 1).

Moreover, clinical studies have found larger carotid-femoral pulse wave velocities (cf-PWVs) in patients with AAA than in age-matched healthy subjects [43-45]. The values of cf-PWV for control and AAA patients reported by three clinical studies are listed in Table 1. From these data a cf-PWV increased of 4.3 m/s was calculated in patients suffering from AAA. This change was considered in the parameter sensitivity analysis by increasing the prescribed desired cf-PWV as described in Charlton *et al.* [14].

Table 1. Carotid-femoral pulse wave velocities (m/s) measured in control cohorts of healthy subjects and in cohorts of patients with AAA.

Control (number)	AAA patient (number)	Reference
10.0 (20)	14.8 (18)	[43]
10.03 (42)	12.99 (108)	[44]
7.97 (31)	13.11 (48)	[45]
9.33	13.63	Mean value

2.3. Database of in silico pulse waves

2.3.1. Modeling a database of pulse waves in subjects with and without an AAA

The entire database of *in silico* PWs created in this study contains three subsets: (i) baseline subset, (ii) increased global stiffness (IGS) subset, and (iii) AAA subset. The first two subsets consist of subjects without AAAs, while the third subset contains subjects with different AAA sizes.

The baseline subset was modeled based on the database developed by Charlton *et al.* [14], which contains six age groups with 729 subjects in each group. In the present study, only the three groups with the older subjects (55, 65, and 75 years old) were used since AAA usually occurs in the elderly rather than the young [2,22]. The baseline subset was obtained by modifying each of the original 2,187 (729×3) subjects as described in Section 2.1. The IGS subset (also 2,187 subjects) was created from the baseline subset, by increasing the desired cf-PWV by 4.3 m/s as described above (see Table 1).

According to the parameter sensitivity analysis, the AAA-related parameters that strongly influence the simulated PWs were AAA maximum diameter and global stiffness of the systemic arteries (see Section 3.1). Variations in global stiffness, which was quantified by cf-PWV, were already considered in the IGS subset. Accordingly, the AAA subset was created by introducing an AAA with maximum diameters of 30, 40, or 50 mm to each subject of the IGS subset. The resulting AAA subset thereby included 6,561 (2,187×3) subjects with three different AAA sizes. The methodology used to simulate an AAA for each subject followed the steps described in Section 2.1 to obtain the baseline subject with an AAA, except for the calculation of AAA local stiffness. Herein, higher *Eh* values with cosine distributions were assigned instead of the constant *Eh* values used in the baseline and IGS subsets.

A literature review provided the elastic modulus, *E*, and wall thickness, *h*, of the normal infrarenal abdominal aorta and AAA, as summarized in Table 2. The mean increase in *E* from normal to AAA was 73.2%. The average *h* increased by 42.9%, from 1.4 mm (normal condition) to 2 mm (AAA) and was found to be independent of AAA size [42]. Accordingly, the *Eh* value of the infrarenal abdominal aorta for the baseline 65-year-old subject in the AAA subset was assigned a cosine distribution with the mean value increasing by 147.43% with respect to the baseline subset. At the two extremes in the vessel, *Eh* was assigned the same values as for the corresponding subject in the IGS subset. All other 6,560 subjects in the AAA subset were prescribed the same distribution of *Eh* in the infrarenal abdominal aorta as the baseline 65-year-old subject. This distribution was linearly scaled to maintain the value at the two vessel extremes used in the IGS subset.

Preprints (www.preprints.org) | NOT PEER-REVIEWED | Posted: 30 March 2021 doi:10.20944/preprints202103.0745.v1

Table 2. Elastic modulus and wall thickness of the normal infrarenal abdominal aorta and AAA.

Source	Value	Reference
Growth ratio of elastic modulus from normal to AAA		
Measured by magnetic resonance elastography	96.8%	[42]
Calculated from the measured pressure and diameter	49.6%	[46]
	73.2%	Mean value
Normal wall thickness		
Derived from clinical measurements	1.4 ~ 1.5 mm	[25]
	1.39 mm	[47]
	1.4 mm	Mean value
AAA wall thickness		
Derived from clinical measurements	2 mm	[37]
	1.63 mm	[48]
	1.48 mm	[49]
	2.71 mm	[50]
	2.87 mm	[51]
	1.64 mm	[52]
Used by previous model-based studies	2 mm	[21], [40]
	2 mm	Mean value

Figure 2 shows the variations in the model input parameters with age for the entire database. These include the cardiovascular parameters prescribed by Charlton *et al.* [14] and the AAA-related parameter changes introduce in this study; *i.e.,* the AAA maximum diameter and global stiffness of the systemic arteries (shown in red dots and lines).

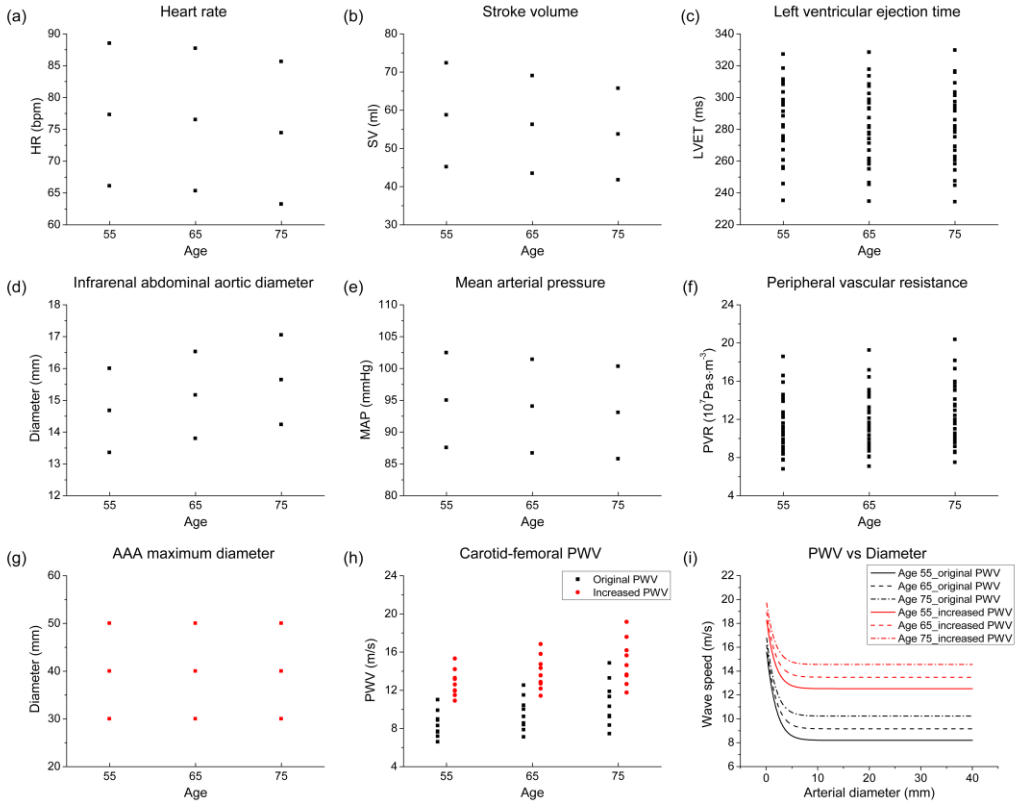

Preprints (www.preprints.org) | NOT PEER-REVIEWED | Posted: 30 March 2021 doi:10.20944/preprints202103.0745.v1

Figure 2. Variations of model parameters used to construct the new database of *in silico* pulse waves. The AAA maximum diameter and increased pulse wave velocity (PWV) values shown in red were added to the original database [14] (with parameters shown in black) to simulate increased stiffness and AAAs. Panel (i) shows the PWV as a function of the arterial diameter for the baseline model of each age, in the baseline (black) and IGS/AAA (red) subsets.

2.3.2. Extracting pulse wave indexes

The cf-PWV and the augmentation index (AIx) have been shown to be significantly higher in patients with AAA compared to normal subjects [43-45]. Accordingly, for each subject in this study, cf-PWV was calculated from the carotid-femoral pulse transit time (cf-PTT) and corresponding arterial path length, with the cf-PTT measured from the pressure PWs in the carotid and femoral arteries using the foot-to-foot method [14,53]. Wave separation analysis [54] was used to calculate the AIx for each virtual subject, as well as the timing and magnitude of wave reflection. The forward (P_f) and backward (P_b) components of the pressure PW in the ascending aorta were calculated from the pressure (P), flow (Q), and local characteristic impedance (Z_c, herein the average value of the modulus of the 3rd to 10th harmonics of the input impedance [55]),

$$\begin{cases} P_f = (P + Z_c Q)/2 \\ P_b = (P - Z_c Q)/2 \end{cases}. \quad (5)$$

Wave reflection magnitude was calculated as the ratio of the amplitude of P_b to the amplitude of P_f. The time delay ($\Delta T_{f\text{-}b}$) between P_b and P_f was obtained using their zero cross-over as reference points. The AIx was calculated as

$$\text{AIx} = 100 \times \frac{\text{SBP} - P_{fb}}{\text{PP}}, \quad (6)$$

with SBP the systolic blood pressure, PP the pulse pressure, and P_{fb} the pressure at the time when the P_b adds to the P_f (corresponding to the zero cross-over of P_b).

The PPG PW in the digital artery of each virtual subject was extracted for further analysis using the mathematical expression [14],

$$\text{PPG}(t) = \int_0^t \left(Q_{1D}(t') - Q_{out}(t') \right) dt', \quad (7)$$

where, Q_{1D} is the inflow to the windkessel segment connecting with the arterial outlet, and Q_{out} is the outflow (see Figure 1).

2.4. Machine learning-based pulse wave analysis

2.4.1. Recurrent neural network

RNN is a machine learning architecture that is widely applied to handle time-series data in which the inputs at each time step include not only the input from the current time step, but also the output from the previous step [56]. For the purpose of improving the accuracy of prediction, bidirectional RNN (BRNN) – an advanced architecture – may be chosen when all time steps of the sequential input data are available [57]. Among the different types of nodes for RNN, the long short-term memory (LSTM) unit is one of the most suitable units for data with long duration, which is able to stop vanishing gradients by keeping track of dependencies between different time steps [58]. Accordingly, BRNN with LSTM was employed to perform the machine learning-based PW analysis in this study. Figure 3 shows a schematic of this machine learning architecture together with the workflow followed to train the machine learning model using the *in silico* PWs from the new database.

Preprints (www.preprints.org) | NOT PEER-REVIEWED | Posted: 30 March 2021 doi:10.20944/preprints202103.0745.v1

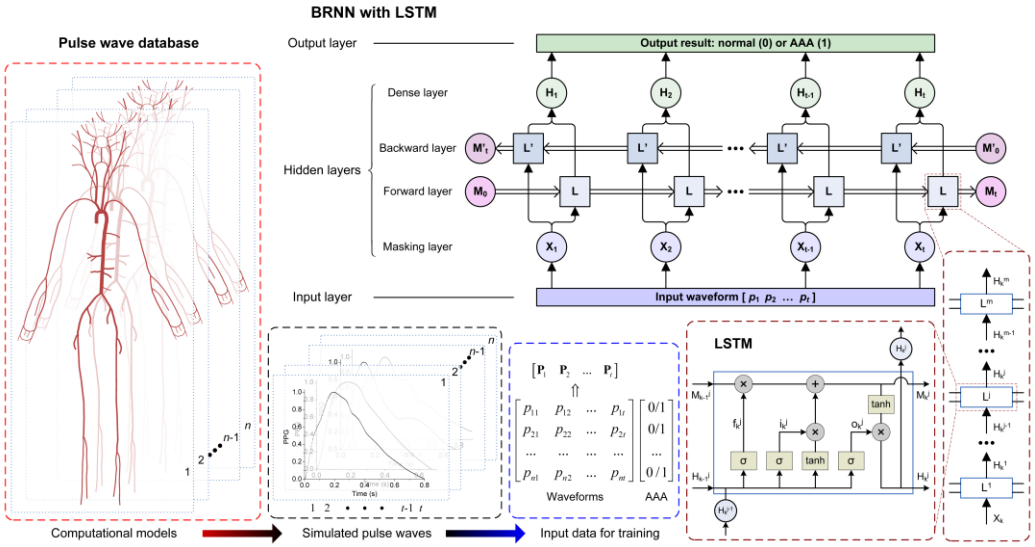

Figure 3. Schematics of the bidirectional recurrent neural network with long short-term memory used in the pulse wave analysis. Simulated PPG waves in n = 8,748 virtual subjects are used as input data for training a BRNN with LSTM (see Equation (8) for the mathematical expressions of a LSTM unit) to predict the presence (output = 1) or not (output = 0) of an AAA. The BRNN contains input, output and hidden layers, each hidden layer consisting of masking, forward, backward, and dense layers. The forward and backward layers include a series of LSTM units.

In the present machine learning architecture, first a batch of PWs were imported into the input layer, where the waves with short durations were extended to the duration of the longest wave by filling dummy values (*i.e.*, the largest floating-point number that the system can support) at the end. Subsequently, the masking layer reacted to exclude the dummy values from being considered when the data were processed in the following layers. After the forward and backward layers processed the time-series data, a dense layer with an activation function (herein the sigmoid function) was used to estimate the output result. The forward and backward layers consisted of a series of LSTM units (see Figure 3), with the structure of each unit described as

$$\begin{cases} f_k^j = \sigma\left(U_f^j H_k^{j-1} + W_f^j H_{k-1}^j + b_f^j\right) \\ i_k^j = \sigma\left(U_i^j H_k^{j-1} + W_i^j H_{k-1}^j + b_i^j\right) \\ o_k^j = \sigma\left(U_o^j H_k^{j-1} + W_o^j H_{k-1}^j + b_o^j\right) \\ M_k^j = f_k^j M_{k-1}^j + i_k^j \tanh\left(U_M^j H_k^{j-1} + W_M^j H_{k-1}^j + b_M^j\right) \\ H_k^j = o_k^j \tanh\left(M_k^j\right) \end{cases}, \tag{8}$$

where H_k^{j-1} and H_k^j are the input and output, respectively, of the kth LSTM unit in the jth layer, and M_k^j is the memory cell. U and W are the weights, and b is the bias. The subscripts f, i, and o represent the forget gate, input gate, and output gate, respectively. σ and tanh represent the sigmoid function and tanh function, respectively. The parameters of the present machine learning architecture are summarized in Table 3. This architecture was constructed using the open-source library TensorFlow 2.1 together with the high-level application programming interface Keras. The development of this architecture referred to a previous study as well as the corresponding online repository [59].

Table 3. Parameters assigned to the BRNN with LSTM.

Parameter	Value
Number of LSTM units	16
Batch size	32

 doi:10.20944/preprints202103.0745.v1

Epoch number	256
Optimizer	Adam
Cost function	Binary cross-entropy

2.4.2. Training and testing

PPG PWs in the digital arteries were extracted from the new database of *in silico* PWs to train and test the machine learning architecture (see Figure 3). The entire database included 10,935 subjects with (6,561) and without (4,374) an AAA, which was randomly split into a training (80%, 8,748) and testing (20%, 2,187) set. The infrarenal abdominal aorta was assigned a label condition of '0' if an AAA was not present and '1' if an AAA was present. The PPG PWs in the training set together with their corresponding conditions were employed in the training process. Subsequently, the trained machine learning model was tested on the testing set to evaluate its performance in the early detection of AAAs (*i.e.*, classification of the normal (0) and AAA (1) conditions). Moreover, the trained machine learning model was further tested on a modified testing set which consisted of randomly varied PPG PWs obtained by superposing random variations (uniform distribution between -50% and 50%) to the first twenty harmonics of each PW. These variations reduced the similarity of the testing set to the training set and made the PWs more realistic by simulating the presence of measurement errors.

3. Results

3.1. Parameter sensitivity analysis

Figure 4 shows the simulated pressure PWs in the infrarenal abdominal aorta, and an upstream (ascending aorta) and downstream (femoral artery) vessel with individual variations in the AAA-related parameters described in Section 2.2. The maximum AAA diameter was the dominant morphological feature affecting the PW shape in these three arteries, introducing oscillations to the baseline PW with their amplitudes increasing with the diameter size. In contrast, the type of AAA shape and AAA length only had small influences on the simulated pulse waveforms (see the first three rows of Figure 4). Arterial stiffness also influenced pulse waveforms (see the last two rows of Figure 4). Although the AAA local stiffness only had a moderate influence, the global stiffness of the larger systemic arteries considerably affected PW morphology. The pulse pressure increased with the stiffening of the vascular wall in all one-dimensional model arteries (global stiffening) under both normal and AAA conditions (see the last row of Figure 4). Under AAA conditions, the increased pulse pressure combined with the oscillations introduced by the localized change in diameter in the infrarenal abdominal aorta.

Preprints (www.preprints.org) | NOT PEER-REVIEWED | Posted: 30 March 2021 doi:10.20944/preprints202103.0745.v1

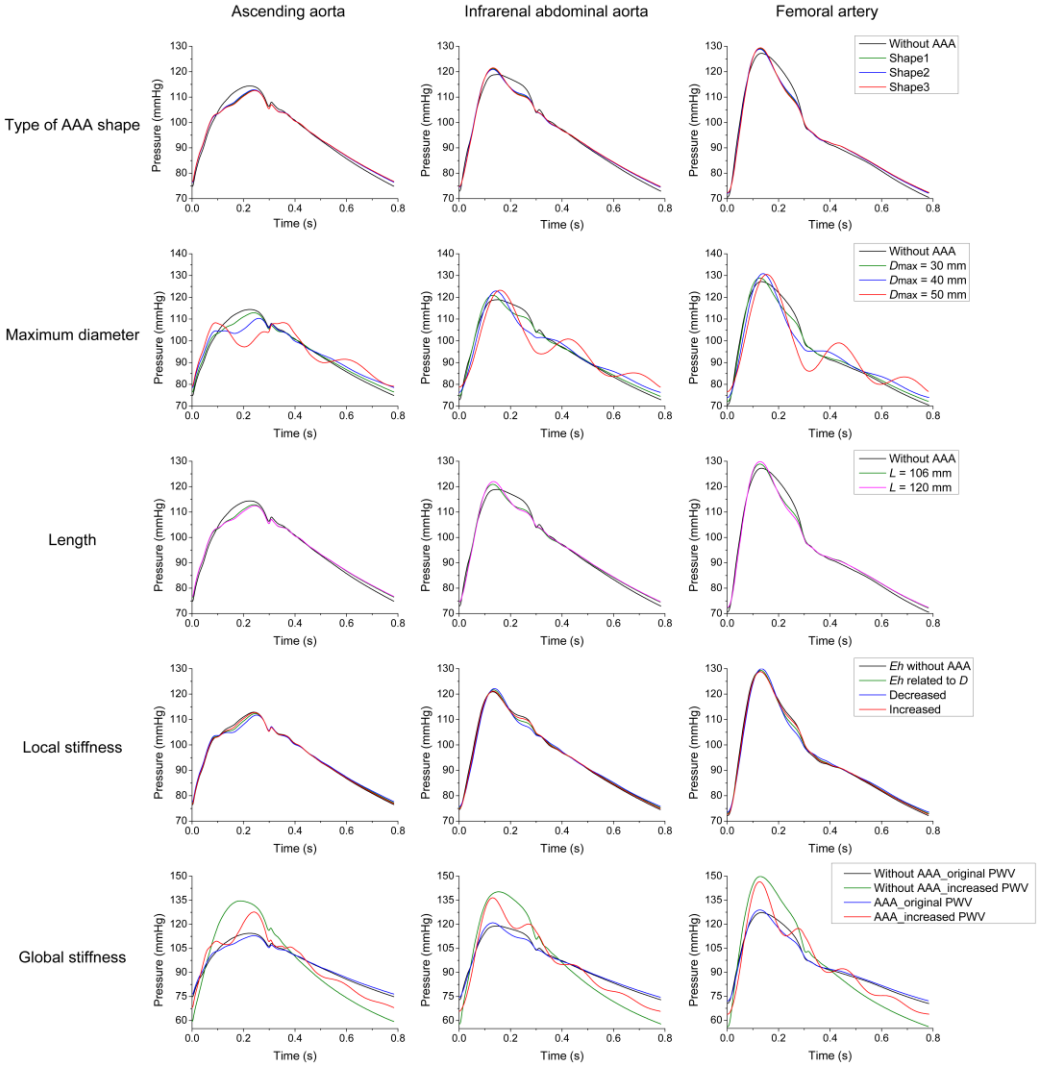

Figure 4. Simulated pressure waveforms in the ascending aorta (left), infrarenal abdominal aorta (middle), and femoral artery (right) with individual variations in the AAA-related parameters indicated at the start of each row and illustrated in Figure 1.

The simulated flow velocity PWs at the same three arterial sites were also mainly affected by changes in maximum AAA diameter and overall stiffness (see Figure 5). However, only the infrarenal abdominal aorta and femoral artery were affected by these changes, since the velocity PW in the ascending aorta was determined primarily by the prescribed inflow waveform at the aortic root and the ascending aorta diameter, and neither was varied to simulate arterial haemodynamics with the presence of an AAA. Furthermore, the amplitude of the velocity PW in the infrarenal abdominal aorta was reduced by more than 50% for all AAA-related parameters, since the AAA increased the luminal cross-sectional area in that vessel without changing the flow rate.

Preprints (www.preprints.org) | NOT PEER-REVIEWED | Posted: 30 March 2021 doi:10.20944/preprints202103.0745.v1

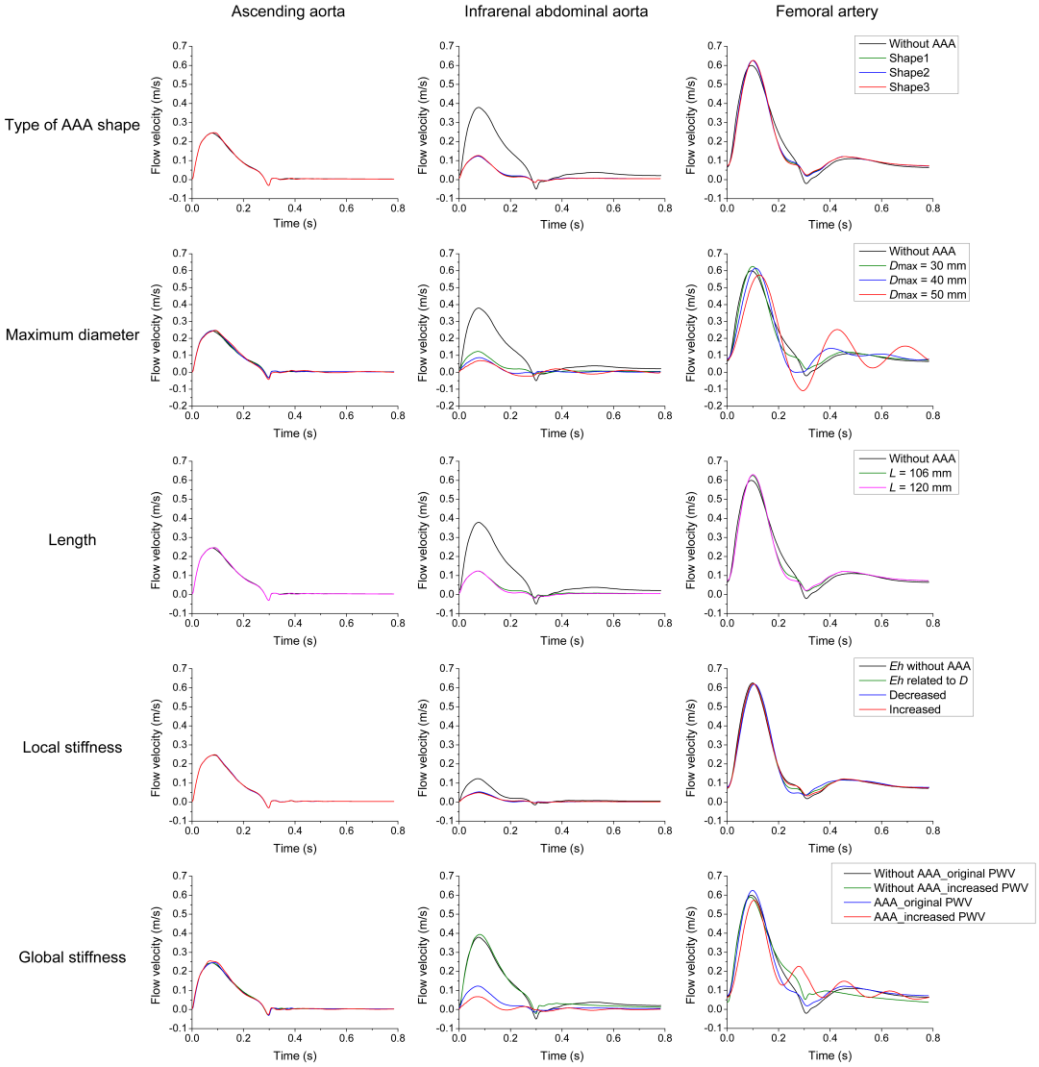

Figure 5. Simulated flow velocity waveforms in the ascending aorta (left), infrarenal abdominal aorta (middle), and femoral artery (right) with individual variations in the AAA-related parameters indicated at the start of each row and illustrated in Figure 1.

3.2. Effects of AAA on pulse waveforms and comparison with the literature

Figure 6 shows pressure, flow velocity, and PPG PWs for the baseline 65-year-old subjects in the IGS and AAA subsets at various measurement sites. The presence of an AAA introduced oscillations to the PWs in the infrarenal abdominal aorta (where the AAA is located), as well as in other upstream and downstream arteries. The amplitudes of these oscillations increased with increasing maximum AAA diameter. Further comparison of the PPG PWs in the digital artery in the frequency domain revealed increasing discrepancies between the magnitudes of the 5th and the 6th harmonics with the increasing maximum AAA diameter. These findings suggest that PWs measured in peripheral sites, such as the digital artery in the finger, could be used to detect the presence of an AAA in clinical practice.

According to *in vivo* measurements reported by previous studies, the flow velocity PW in a normal infrarenal abdominal aorta has a triphasic waveform due to the highly resistive blood flow, while the AAA leads to a much slower and less resistive waveform [8]. These results were qualitatively comparable with the simulated velocity PWs in the middle of the infrarenal abdominal aorta shown in Figure 6. Moreover, *in vitro* measurements in a hydraulic bench model showed similar trends to the simulated results of the present study, such as the oscillations in the pressure PW in the ascending aorta with

Preprints (www.preprints.org) | NOT PEER-REVIEWED | Posted: 30 March 2021 doi:10.20944/preprints202103.0745.v1

an AAA in the infrarenal abdominal aorta, and the increased magnitude and oscillations in the velocity PW at the inlet of the AAA [36].

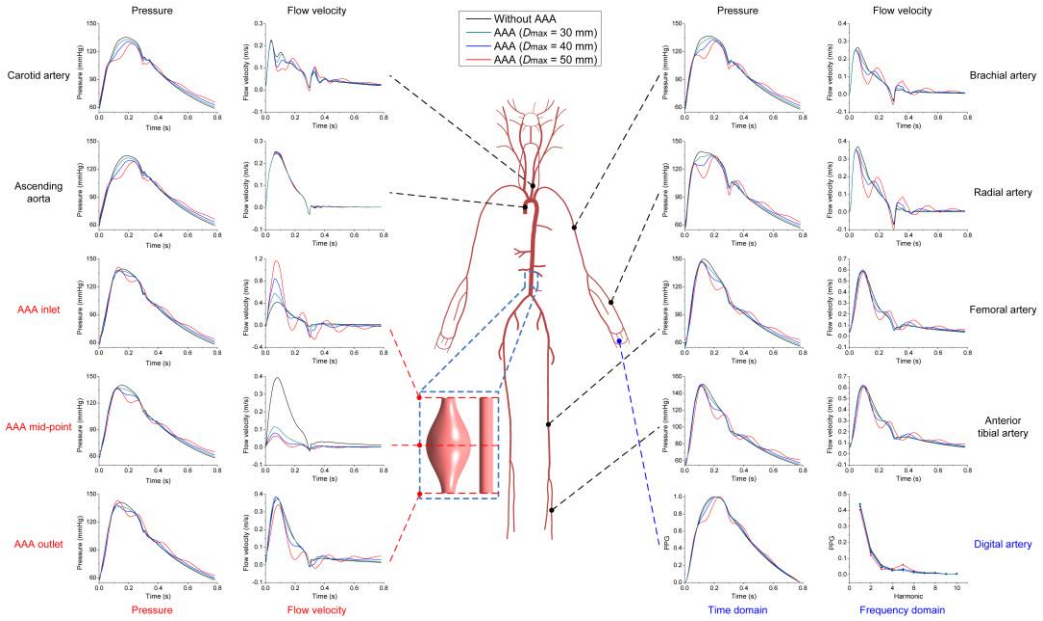

Figure 6. Simulated pressure and flow velocity pulse waves at the infrarenal abdominal aorta (labeled in red) and other common measurement sites (labeled in black) for the baseline 65-year-old subject in the IGS subset (without AAA) and AAA subset (D_{max} = 30 mm, D_{max} = 40 mm, and D_{max} = 50 mm). The PPG wave is shown in the digital artery in the time and frequency domains (labeled in blue).

3.3. Comparison of pulse wave indexes extracted from the pulse wave database

Figure 7 compares PW indexes obtained under normal conditions (baseline and IGS subsets) and with an AAA (AAA subset) from pressure measurements in the ascending aorta (except for cf-PWV and digital PPG indexes). These indexes were selected because they have been shown to differ in subjects with and without AAA in clinical studies [43-45]. The mean blood pressure (MBP) in the ascending aorta was similar between the two conditions, but the systolic blood pressure (SBP) increased in the IGS and AAA subsets and the diastolic blood pressure (DBP) decreased due to arterial wall stiffening increasing pulse pressure (Figure 7 (a), (b), (c)), as well as carotid-femoral pulse wave velocity (Figure 7 (g)) . Moreover, although the wave reflection magnitude (P_b/P_f) was similar between the IGS and AAA subsets, the wave reflection time ($\Delta T_{f\text{-}b}$) increased significantly in the AAA condition (Figure 7 (d) and (e)). The AIx did not show a clear trend, though it was considerably higher in the AAA subset with the largest AAA diameters than in the baseline subset (Figure 7 (f)).

Indexes calculated from the peripheral PW were also considered in this study. The differences between the magnitudes of the 5th and the 6th harmonics of the PPG PWs in the digital artery, which showed a significant increase with the presence of an AAA in the baseline 65-year-old subject (see Figure 6, last plot), were compared among different subsets. As shown in Figure 7 (h) and (i), the mean value of the differences in magnitude were similar among different subsets, but the standard deviations of the AAA subset were relatively larger, indicating a wide range of values in the AAA subset. This result suggests that the difference between the magnitudes of the 5th and the 6th harmonics of the digital PPG PW (as well as the PW itself) was strongly influenced by various cardiovascular parameters in addition to the AAA size. Therefore, the detection of an AAA by individual analysis of PPG PW indexes is a challenging task.

Preprints (www.preprints.org) | NOT PEER-REVIEWED | Posted: 30 March 2021 doi:10.20944/preprints202103.0745.v1

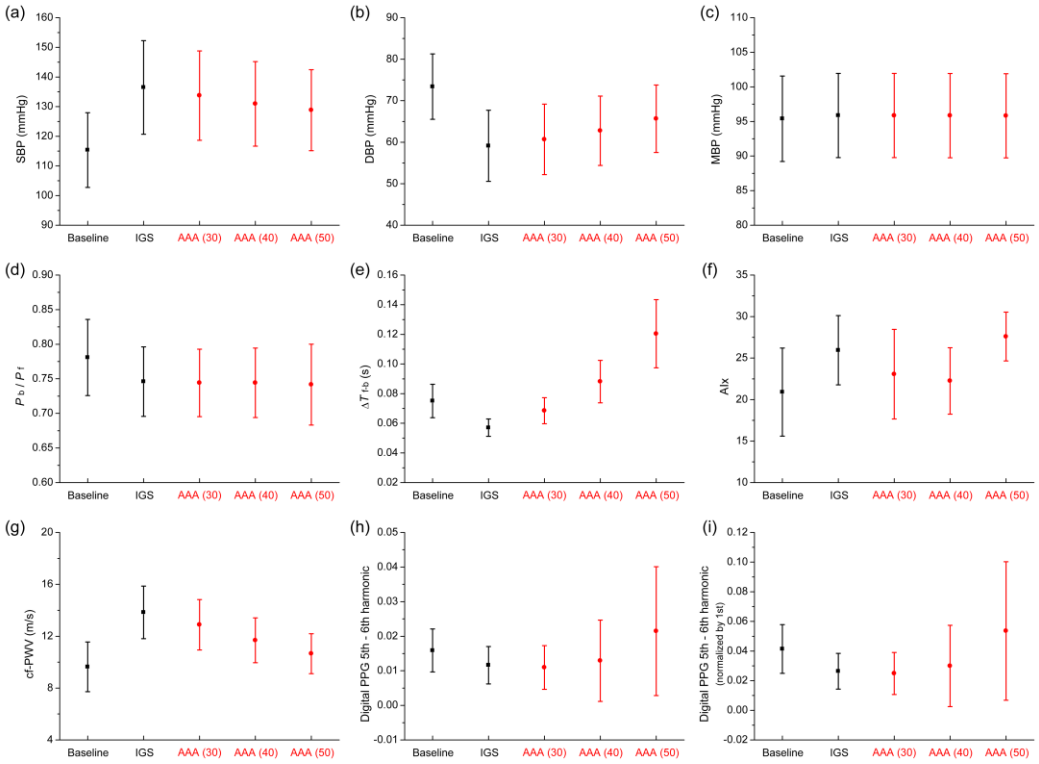

Figure 7. Comparison of pulse wave indexes obtained in the baseline and increased global stiffness (IGS) subsets (in black) and the AAA subset with different AAA sizes (in red). Dots indicate mean values and error bars represent standard deviations. SBP: systolic blood pressure; DBP: diastolic blood pressure; MBP: mean blood pressure; P_b/P_f: wave reflection magnitude; $\Delta T_{f\text{-}b}$: time delay between P_b and P_f; AIx: augmentation index; cf-PWV: carotid-femoral pulse wave velocity. All indexes were calculated in the ascending aorta except for cf-PWV and digital PPG indexes.

3.4. AAA early detection using machine learning

Figure 8 shows the confusion matrices and receiver operator characteristic (ROC) curves of the AAA prediction using both the original testing set (top) and the modified testing set with randomly varied PPG PWs (bottom). The trained machine learning model showed perfect performance when using the original set. The area under the curve (AUC) was approximately equal to 1, and almost all subjects were classified correctly (see top panels in Figure 8). When the modified testing set was employed, the resulting AUC could reach 0.928, suggesting that the trained machine learning model was competent to classify normal and AAA conditions using digital PPG PWs that had less resemblance to the PWs of the training set.

Further analysis of the type of subjects in each condition of the confusion matrix revealed that misdiagnosis (*i.e.*, false positive) usually occurred in older subjects (age 75: 89%, when using the original testing set; 53%, when using the modified testing set), while younger subjects with relatively smaller AAA were more likely to suffer from missed diagnosis (*i.e.*, false negative) (see central column in Figure 8). Nonetheless, the ratio of misdiagnosis and missed diagnosis were overall low in the predicted results using both the original and modified testing sets (misdiagnosis: 9/853 (original), 117/853 (modified); missed diagnosis: 13/1334 (original), 176/1334 (modified)). These findings suggest that the machine learning model trained with a database of *in silico* PWs could be used for early detection of AAAs in real subjects.

Preprints (www.preprints.org) | NOT PEER-REVIEWED | Posted: 30 March 2021 doi:10.20944/preprints202103.0745.v1

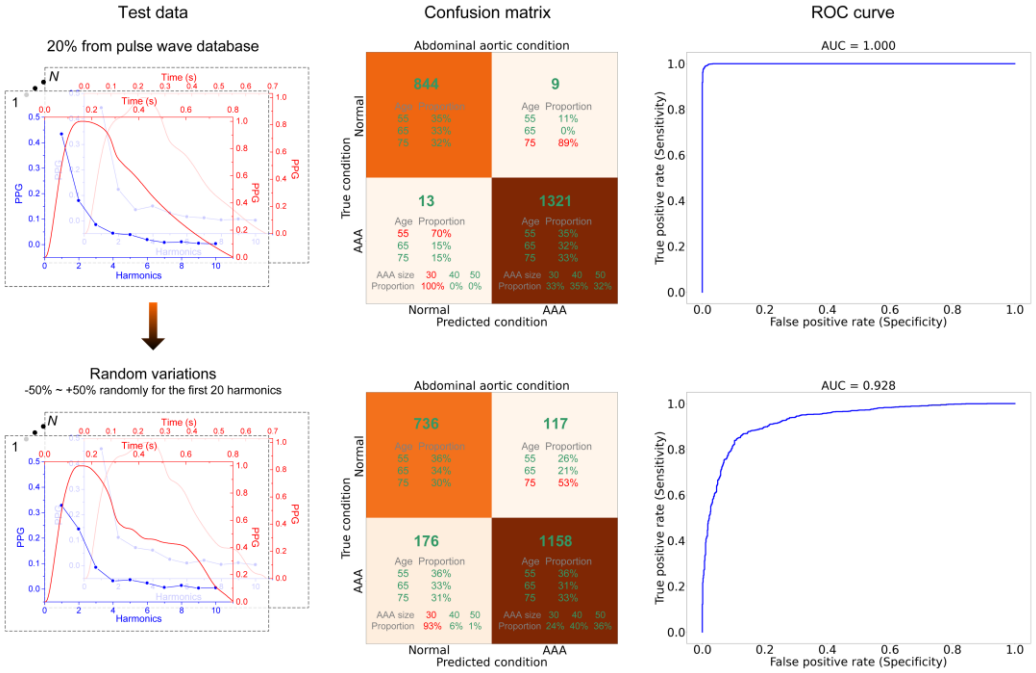

Figure 8. Performance of the trained machine learning model for the early detection of AAAs. Test data (left), confusion matrix (middle), and ROC curve (right) when testing in the original (top) and modified (bottom) testing sets. The confusion matrices indicate the number of subjects in each condition together with the proportion of each age and AAA size (if applicable) in green or red.

4. Discussion

We have provided a proof of concept for the feasibility of early detection of AAAs by machine learning-based pulse wave (PW) analysis. Given the high mortality of AAA rupture, early detection of AAAs is crucial for an effective treatment to reduce the risk of rupture. AAAs are often detected as incidental findings of medical imaging assessments which are costly and can only be performed at specialised centres. Analysis of PPG PWs, on the other hand, offers the possibility to screen the wider population, since these signals can be acquired by a wide range of ubiquitous devices such as smartphones, tablets, and fitness devices. Using a newly created database of *in silico* PWs in subjects with and without AAAs, we have demonstrated that AAA detection using individual PW indexes is a challenging task, but machine learning-based PW analysis is a more promising approach. By using a recurrent neural network we have obtained a sensitivity in AAA detection of 86.8% and a specificity of 86.3% when tested in a modified dataset representative of a sample of subjects with and without AAAs with random noise added to their PPG PWs.

The database of *in silico* PWs was created using a physics-based computational blood flow model, which allowed us to study the interpretability of the machine learning results. The simulated AAAs in the virtual subjects of the database covered a range of AAA sizes – from small to moderate – which enabled evaluation of the ability of the machine learning model to predict the presence of an AAA in its early stage of development. The size of an AAA is usually quantified by the maximum diameter which, according to the results of our parameter sensitivity analysis, is the major morphological factor influencing PWs. This finding is consistent with the fact that many computational model-based studies simulating PWs in the presence of AAAs have varied the AAA maximum diameter [10,33,36]. In addition, the virtual subjects in our new database had their global stiffness increased to make the simulated PWs more realistic. Many clinical studies have observed an increase in the overall stiffness of patients with an AAA [43-45], although this has not been considered in previous computational model-based studies investigating the influence of AAAs on PW propagation [10,33-36]. Our parameter sensitivity analysis has suggested that the global stiffness of large systemic arteries

has a considerable effect on the discrepancies of the PWs under normal and AAA conditions, highlighting the importance of simulating the effect of increased global stiffness with AAAs. Moreover, the false positive and false negative results of the machine learning prediction were closely related to the age of the subject and AAA size, suggesting that these two factors should be considered to optimize the predictive power of machine learning algorithms. Lastly, although the PPG PW was used in the training and testing of the machine learning architecture used in this study, PWs measured along the arteries in the arm were similarly affected by the presence of an AAA. As a result, it is expected that any of these PWs could be used for AAA detection by machine learning-based PW analysis, although the PPG PW at the digital artery or radial artery may be easier to acquire in real subjects.

The findings of this study must be considered in the context of certain limitations. Firstly, the computational model used in the present study is a one-dimensional model rather than a three-dimensional model that should be more accurate in simulating blood flow in the presence of an AAA. Nonetheless, a recent study has demonstrated that one-dimensional modelling of the large arteries is accurate compared to three-dimensional modelling to simulate PW propagation across AAA [60]. Secondly, in patients with AAAs, calcification and intraluminal thrombus usually occur within the AAA, which change the stiffness (both the elastic modulus and wall thickness) of the AAA and significantly influence the distribution of AAA wall stresses [61-63]. However, one-dimensional modelling is not able to directly simulate calcification and intraluminal thrombus. In this study, the effects of calcification and intraluminal thrombus were described by increasing the local stiffness of AAAs, which was also the approach adopted by previous studies using one-dimensional modelling [10,35,36]. Lastly, although the variations of many influential cardiovascular parameters were considered to generate the present *in silico* PW database, the conditions of real subjects were not fully described since they are more complicated and not so systematic. The testing set was derived from the *in silico* PW database and *in vivo* measurements were not used, making our study a proof-of-concept. Further research is warranted to test the machine learning model trained in this study using PPG PWs measured in real subjects.

A well trained and tested machine learning model would be a very useful mathematical tool for the early detection of AAAs by pulse wave analysis. The proliferation of commercial wearable devices that can accurately measure PPG signals on the wrist or finger offers an opportunity to screen the wider population for AAAs in daily life. AAA diagnosis should be ultimately confirmed by a medical imaging examination. However, AAA detection by PPG PW analysis may help improve AAA diagnosis by identifying those subjects with a potential AAA, thus paving the way for more effective treatment that reduces current mortality rates.

Author Contributions: Conceptualization, Tianqi Wang and Jordi Alastruey; methodology, Tianqi Wang, Weiwei Jin and Jordi Alastruey; data analysis, Tianqi Wang, Fuyou Liang and Jordi Alastruey; writing—original draft preparation, Tianqi Wang; writing—review and editing, Jordi Alastruey; project administration, Jordi Alastruey. All authors have read and agreed to the published version of the manuscript.

Funding: This research was funded by the Wellcome EPSRC Centre for Medical Engineering at King's College London [WT 203148/Z/16/Z], Department of Health through the National Institute for Health Research (NIHR) Cardiovascular MedTech Co-operative at Guy's and St Thomas' NHS Foundation Trust (GSTT), and the Ministry of Science and Higher Education of the Russian Federation within the framework of state support for the creation and development of World-Class Research Centers Digital biodesign and personalized healthcare [075-15-2020-926]. TW was funded by the China Scholarship Council [201906230032]. WJ was funded by a King's College London PGR International Scholarship. FL was funded by the National Natural Science Foundation of China [11972231]. JA was funded by the British Heart Foundation (BHF) [PG/15/104/31913].

Data Availability Statement: The data presented in this study are available in haemod.uk/aaa.

Conflicts of Interest: The authors declare no conflict of interest. The funders had no role in the design of the study; in the collection, analyses, or interpretation of data; in the writing of the manuscript, or in the decision to publish the results.

References

1. Sakalihasan, N.; Limet, R.; Defawe, O.D. Abdominal aortic aneurysm. *Lancet* **2005**, *365*, 1577–1589.
2. Golledge, J.; Muller, J.; Daugherty, A.; Norman, P. Abdominal aortic aneurysm: pathogenesis and implications for management. *Arteriosclerosis, Thrombosis, and Vascular Biology* **2006**, *26*, 2605–2613.
3. Scott, R.A.P.; Ashton, H.A.; Kay, D.N. Abdominal aortic aneurysm in 4237 screened patients: prevalence, development and management over 6 years. *British Journal of Surgery* **1991**, *78*, 1122–1125.
4. Kent, K.C. Abdominal aortic aneurysms. *The New England Journal of Medicine* **2014**, *371*, 2101–2108.
5. Upchurch, G.R.; Schaub, T.A. Abdominal aortic aneurysm. *American Family Physician* **2006**, *73*, 1198–1204.
6. Aggarwal, S.; Qamar, A.; Sharma, V.; Sharma, A. Abdominal aortic aneurysm: a comprehensive review. *Experimental and Clinical Cardiology* **2011**, *16*, 11–15.
7. Wells, C.E.; Pugh, N.D.; Woodcock, J.P. Abdominal aortic aneurysm detection by common femoral artery Doppler ultrasound waveform analysis. *Journal of Medical Engineering & Technology* **2011**, *35*, 34–39.
8. Wood, M.M.; Romine, L.E.; Lee, Y.K.; Richman, K.M.; O'Boyle, M.K.; Paz, D.A.; Chu, P.K.; Pretorius, D.H. Spectral doppler signature waveforms in ultrasonography: a review of normal and abnormal waveforms. *Ultrasound Quarterly* **2010**, *26*, 83–99.
9. Elgendi, M. *PPG Signal Analysis: An Introduction Using MATLAB®*; CRC Press: 2020.
10. Chakshu, N.K.; Sazonov, I.; Nithiarasu, P. Towards enabling a cardiovascular digital twin for human systemic circulation using inverse analysis. *Biomechanics and Modeling in Mechanobiology* **2020**, https://doi.org/10.1007/s10237-10020-01393-10236.
11. Tavallali, P.; Razavi, M.; Pahlevan, N.M. Artifcial intelligence estimation of carotid-femoral pulse wave velocity using carotid waveform. *Scientific Reports* **2018**, *8*, 1014.
12. Biswas, D.; Everson, L.; Liu, M.; Panwar, M.; Verhoef, B.-E.; Patki, S.; Kim, C.H.; Acharyya, A.; Van Hoof, C.; Konijnenburg, M., et al. CorNET: deep learning framework for PPG-based heart rate estimation and biometric identification in ambulant environment. *IEEE Transactions on Biomedical Engineering* **2019**, *13*, 282–291.
13. Jones, G.; Parr, J.; Nithiarasu, P.; Pant, S. Machine learning for detection of stenoses and aneurysms: application in a physiologically realistic virtual patient database. *arXiv* **2021**, *2103.00599*.
14. Charlton, P.H.; Harana, J.M.; Vennin, S.; Li, Y.; Chowienczyk, P.; Alastruey, J. Modelling arterial pulse waves in healthy ageing: a database for in silico evaluation of haemodynamics and pulse wave indexes. *American Journal of Physiology. Heart and Circulatory Physiology* **2019**, *317*, H1062–H1085.
15. Jones, G.; Parr, J.; Nithiarasu, P.; Pant, S. A physiologically realistic virtual patient database for the study of arterial haemodynamics. *arXiv* **2021**, *2102.10655*.
16. Wang, T.; Liang, F.; Li, L.; Zhang, W.; Wang, G.; Wang, J.; Zhang, C.; Qi, X. A computational model-based study on the exchangeability of hepatic venous pressure gradients measured in multiple hepatic vein. *Medical Engineering and Physics* **2020**, *84*, 28–35.
17. Wang, T.; Liang, F.; Zhou, Z.; Qi, X. Global sensitivity analysis of hepatic venous pressure gradient (HVPG) measurement with a stochastic computational model of the hepatic circulation. *Computers in Biology and Medicine* **2018**, *97*, 124–136.
18. Vilalta, G.; Nieto, F.; Vaquero, C.; Vilalta, J.A. Quantitative indicator of abdominal aortic aneurysm rupture risk based on its geometric parameters. *World Academy of Science, Engineering and Technology* **2010**, *70*, 181–185.

19. Giannoglou, G.; Giannakoulas, G.; Soulis, J.; Chatzizisis, Y.; Perdikides, T.; Melas, N.; Parcharidis, G.; Louridas, G. Predicting the risk of rupture of abdominal aortic aneurysms by utilizing various geometrical parameters revisiting the diameter criterion *Angiology* **2006**, *57*, 487–494.
20. Li, Z.; Kleinstreuer, C. A new wall stress equation for aneurysm-rupture prediction. *Annals of Biomedical Engineering* **2005**, *33*, 209–213.
21. Venkatasubramaniam, A.K.; Fagan, M.J.; Mehta, T.; Mylankal, K.J.; Ray, B.; Kuhan, G.; Chetter, I.C.; McCollum, P.T. A comparative study of aortic wall stress using finite element analysis for ruptured and non-ruptured abdominal aortic aneurysms. *European Journal of Vascular and Endovascular Surgery* **2004**, *28*, 168–176.
22. Lindquist Liljeqvist, M.; Hultgren, R.; Siika, A.; Gasser, T.C.; Roy, J. Gender, smoking, body size, and aneurysm geometry influence the biomechanical rupture risk of abdominal aortic aneurysms as estimated by finite element analysis. *Journal of Vascular Surgery* **2017**, *65*, 1014–1022.
23. Volokh, K.Y.; Vorp, D.A. A model of growth and rupture of abdominal aortic aneurysm. *Journal of Biomechanics* **2008**, *41*, 1015–1021.
24. Grytsan, A.; Watton, P.N.; Holzapfel, G.A. A thick-walled fluid–solid-growth model of abdominal aortic aneurysm evolution: application to a patient-specific geometry. *Journal of Biomechanical Engineering* **2015**, *137*, 031008.
25. Humphrey, J.D.; Holzapfel, G.A. Mechanics, mechanobiology, and modeling of human abdominal aorta and aneurysms. *Journal of Biomechanics* **2012**, *45*, 805–814.
26. Figueroa, C.A.; Taylor, C.A.; Yeh, V.; Chiou, A.J.; Zarins, C.K. Effect of curvature on displacement forces acting on aortic endografts: a 3-dimensional computational analysis. *Journal of Endovascular Therapy* **2009**, *16*, 284–294.
27. Gindre, J.; Bel-Brunon, A.; Kaladji, A.; Duménil, A.; Rochette, M.; Lucas, A.; Haigron, P.; Combescure, A. Finite element simulation of the insertion of guidewires during an EVAR procedure: example of a complex patient case, a first steptoward patient-specific parameterized models. *International Journal for Numerical Methods in Biomedical Engineering* **2015**, *31*, e02716.
28. Casciaro, M.E.; Alfonso, M.A.; Craiem, D.; Alsac, J.M.; El-Batti, S.; Armentano, R.L. Predicting the effect on pulse wave reflection of different endovascular repair techniques in abdominal aortic aneurysm using 1D patient-specific models. *Health and Technology* **2016**, *6*, 173–179.
29. Fraser, K.H.; Meagher, S.; Blake, J.R.; Easson, W.J.; Hoskins, P.R. Characterization of an abdominal aortic velocity waveform in patients with abdominal aortic aneurysm. *Ultrasound in Medicine and Biology* **2008**, *34*, 73–80.
30. Taylor, C.A.; Cheng, C.P.; Espinosa, L.A.; Tang, B.T.; Parker, D.; Herfkens, R.J. In vivo quantification of blood flow and wall shear stress in the human abdominal aorta during lower limb exercise. *Annals of Biomedical Engineering* **2002**, *30*, 402–408.
31. Les, A.S.; Yeung, J.J.; Schultz, G.M.; Herfkens, R.J.; Dalman, R.L.; Taylor, C.A. Supraceliac and infrarenal aortic flow in patients with abdominal aortic aneurysms: mean flows, waveforms, and allometric scaling relationships. *Cardiovascular Engineering and Technology* **2010**, *1*, 39–51.
32. Wang, T.; Alastruey, J.; Liang, F. A computational model-based study on the effect of abdominal aortic aneurysm on pulse wave morphology. *Artery Research* **2020**, *26*, S10–S11.
33. Sazonov, I.; Khir, A.W.; Hacham, W.S.; Boileau, E.; Carson, J.M.; van Loon, R.; Ferguson, C.; Nithiarasu, P. A novel method for non-invasively detecting the severity and location of aortic aneurysms. *Biomechanics and Modeling in Mechanobiology* **2017**, *16*, 1225–1242.
34. Safaei, S. Simulating blood flow in an anatomical arterial network. University of Auckland, 2015.
35. Low, K.; van Loon, R.; Sazonov, I.; Bevan, R.L.T.; Nithiarasu, P. An improved baseline model for a human arterial network to study the impact of aneurysms on pressure-flow waveforms. *International Journal for Numerical Methods in Biomedical Engineering* **2012**, *28*, 1224–1246.

36. Swillens, A.; Lanoye, L.; De Backer, J.; Stergiopulos, N.; Verdonck, P.R.; Vermassen, F.; Segers, P. Effect of an abdominal aortic aneurysm on wave reflection in the aorta. *IEEE Transactions on Biomedical Engineering* **2008**, *55*, 1602–1611.
37. Tong, J.; Cohnert, T.; Holzapfel, G.A. Diameter-related variations of geometrical, mechanical, and mass fraction data in the anterior portion of abdominal aortic aneurysms. *European Journal of Vascular and Endovascular Surgery* **2015**, *49*, 262–270.
38. Martufi, G.; Di Martino, E.S.; Amon, C.H.; Muluk, S.C.; Finol, E.A. Three-dimensional geometrical characterization of abdominal aortic aneurysms: image-based wall thickness distribution. *Journal of Biomechanical Engineering* **2009**, *131*, 061015.
39. Rodríguez, J.F.; Ruiz, C.; Doblaré, M.; Holzapfel, G.A. Mechanical stresses in abdominal aortic aneurysms influence of diameter, asymmetry, and material anisotropy. *Journal of Biomechanical Engineering* **2008**, *130*, 021023.
40. Doyle, B.J.; Morris, L.G.; Callanan, A.; Kelly, P.; Vorp, D.A.; McGloughlin, T.M. 3D reconstruction and manufacture of real abdominal aortic aneurysms: from CT scan to silicone model. *Journal of Biomechanical Engineering* **2008**, *130*, 034501.
41. Shum, J.; Martufi, G.; Di Martino, E.; Washington, C.B.; Grisafi, J.; Muluk, S.C.; Finol, E.A. Quantitative assessment of abdominal aortic aneurysm geometry. *Annals of Biomedical Engineering* **2011**, *39*, 277–286.
42. Kolipaka, A.; Illapani, V.S.P.; Kenyhercz, W.; Dowell, J.D.; Go, M.R.; Starr, J.E.; Vaccaro, P.S.; White, R.D. Quantification of abdominal aortic aneurysm stiffness using magnetic resonance elastography and its comparison to aneurysm diameter. *Journal of Vascular Surgery* **2016**, *64*, 966–974.
43. Durmus, I.; Kazaz, Z.; Altun, G.; Cansu, A. Augmentation index and aortic pulse wave velocity in patients with abdominal aortic aneurysms. *International Journal of Clinical and Experimental Medicine* **2014**, *7*, 421–425.
44. Kadoglou, N.P.E.; Papadakis, I.; Moulakakis, K.G.; Ikonomidis, I.; Alepaki, M.; Moustardas, P.; Lampropoulos, S.; Karakitsos, P.; Lekakis, J.; Liapis, C.D. Arterial stiffness and novel biomarkers in patients with abdominal aortic aneurysms. *Regulatory Peptides* **2012**, *179*, 50–54.
45. Kadoglou, N.P.E.; Moulakakis, K.G.; Papadakis, I.; Ikonomidis, I.; Alepaki, M.; Lekakis, J.; Liapis, C.D. Changes in aortic pulse wave velocity of patients undergoing endovascular repair of abdominal aortic aneurysms. *Journal of Endovascular Therapy* **2012**, *19*, 661–666.
46. Länne, T.; Sonesson, B.; Bergqvist, D.; Bengtsson, H.; Gustafsson, D. Diameter and compliance in the male human abdominal aorta: influence of age and aortic aneurysm. *European Journal of Vascular Surgery* **1992**, *6*, 178–184.
47. Schriefl, A.J.; Zeindlinger, G.; Pierce, D.M.; Regitnig, P.; Holzapfel, G.A. Determination of the layer-specific distributed collagen fibre orientations in human thoracic and abdominal aortas and common iliac arteries. *Journal of the Royal Society Interface* **2012**, *9*, 1275–1286.
48. Shum, J.; Dimartino, E.S.; Goldhammer, A.; Goldman, D.H.; Acker, L.C.; Patel, G.; Ng, J.H.; Martufi, G.; Finol, E.A. Semiautomatic vessel wall detection and quantification of wall thickness in computed tomography images of human abdominal aortic aneurysms. *Medical Physics* **2010**, *37*, 638–648.
49. Raghavan, M.L.; Kratzberg, J.; de Tolosa, E.M.C.; Hanaoka, M.M.; Walker, P.; da Silva, E.S. Regional distribution of wall thickness and failure properties of human abdominal aortic aneurysm. *Journal of Biomechanics* **2006**, *39*, 3010–3016.
50. Martufi, G.; Satriano, A.; Moore, R.D.; Vorp, D.A.; Di Martino, E.S. Local quantification of wall thickness and intraluminal thrombus offer insight into the mechanical properties of the aneurysmal aorta. *Annals of Biomedical Engineering* **2015**, *43*, 1759–1771.
51. Di Martino, E.S.; Bohra, A.; Vande Geest, J.P.; Gupta, N.; Makaroun, M.S.; Vorp, D.A. Biomechanical properties of ruptured versus electively repaired abdominal aortic aneurysm wall tissue. *Journal of Vascular Surgery* **2006**, *43*, 570–576.
52. Shum, J.; Xu, A.; Chatnuntawech, I.; Finol, E.A. A framework for the automatic generation of surface topologies for abdominal aortic aneurysm models. *Annals of Biomedical Engineering* **2011**, *39*, 249–259.
53. Gaddum, N.R.; Alastruey, J.; Beerbaum, P.; Chowienczyk, P.; Schaeffter, T. A technical assessment of pulse wave velocity algorithms applied to Non-invasive arterial waveforms. *Annals of Biomedical Engineering* **2013**, *41*, 2617–2629.

54. Segers, P.; Rietzschel, E.R.; De Buyzere, M.L.; De Bacquer, D.; Van Bortel, L.M.; De Backer, G.; Gillebert, T.C.; Verdonck, P.R. Assessment of pressure wave reflection: getting the timing right! *Physiological Measurement* **2007**, *28*, 1045–1056.
55. Westerhof, N.; Sipkema, P.; van den Bos, G.C.; Elzinga, G. Forward and backward waves in the arterial system. *Cardiovascular Research* **1972**, *6*, 648–656.
56. Schmidhuber, J. Deep learning in neural networks: an overview. *Neural Networks* **2015**, *61*, 85–117.
57. Lipton, Z.C.; Berkowitz, J.; Elkan, C. A critical review of recurrent neural networks for sequence learning. *Computer Science* **2015**, 1–38.
58. Hochreiter, S.; Schmidhuber, J. Long short-term memory. *Neural Computation* **1997**, *9*, 1735–1780.
59. Jin, W.; Chowienczyk, P.; Alastruey, J. Estimating pulse wave velocity from the radial pressure wave using machine learning algorithms. *medRxiv* **2020**, *2020.11.29.20239962*.
60. Jin, W.; Alastruey, J. Arterial pulse wave propagation across stenoses and aneurysms: assessment of 1-D simulations against 3-D simulations and in vitro measurements. *Journal of the Royal Society Interface* **2021**.
61. Li, Z.-Y.; U-King-Im, J.; Tang, T.Y.; Soh, E.; See, T.C.; Gillard, J.H. Impact of calcification and intraluminal thrombus on the computed wall stresses of abdominal aortic aneurysm. *Journal of Vascular Surgery* **2008**, *47*, 928–935.
62. Di Martino, E.S.; Vorp, D.A. Effect of variation in intraluminal thrombus constitutive properties on abdominal aortic aneurysm wall stress. *Annals of Biomedical Engineering* **2003**, *31*, 804–809.
63. Tong, J.; Cohnert, T.; Regitnig, P.; Holzapfel, G.A. Effects of age on the elastic properties of the intraluminal thrombus and the thrombus-covered wall in abdominal aortic aneurysms: biaxial extension behaviour and material modelling. *European Journal of Vascular and Endovascular Surgery* **2011**, *42*, 207–219.